

1           Large-scale properties of clustered networks:  
2                           Implications for disease dynamics

3                           Darren M. Green<sup>a\*</sup> & Istvan Z. Kiss<sup>b</sup>

4   March 26, 2010

5           <sup>a</sup> *Institute of Aquaculture, University of Stirling, Stirling, Stirlingshire FK9 4LA, UK.*

6           <sup>b</sup> *Department of Mathematics, University of Sussex, Falmer, Brighton BN1 9RF, UK.*

7           \* Tel: +44 1786 467872; Fax: +44 1786 472133.

8           *E-mail address: darren.green@stir.ac.uk (D.M. Green).*

9

**Abstract**

10 We consider previously proposed procedures for generating clustered networks and  
11 investigate how these procedures lead to differences in network properties other than  
12 clustering. We interpret our findings in terms of the effect of the network structure on  
13 disease outbreak threshold and disease dynamics. To generate null-model networks for  
14 comparison, we implement an assortativity-conserving rewiring algorithm that alters the  
15 level of clustering while causing minimal impact on other properties. We show that  
16 many theoretical network models used to generate networks with a particular property  
17 often lead to significant changes in network properties other than that of interest. For  
18 high levels of clustering, different procedures lead to networks that differ in degree  
19 heterogeneity and assortativity, and in broader-scale measures such as  $\mathcal{R}_0$  and the  
20 distribution of shortest path lengths. Hence, care must be taken when investigating the  
21 implications of network properties for disease transmission or other dynamic process  
22 that the network supports.

23 *Keywords: Networks, Clustering, Epidemic Dynamics, Percolation*

## 24 **1 Introduction**

25 Contact networks are a frequently used tool in epidemiological modelling: Each  
26 epidemiological unit (be it a person, animal, self-contained sub-population) is considered as  
27 a network *node*, with potentially infectious contact between nodes represented by  
28 directionless *edges* or directed *arcs*. The power of the approach is that by explicitly  
29 considering the pairwise interactions between units, one can extend the results obtained  
30 from compartmental, mean-field, spatial, and metapopulation or household-based models.–  
31 Direction, strength, and (potentially) timing of contact can all be accounted for. In STI  
32 models (Anderson & Garnett, 2000), contact heterogeneity and patterns of connectivity can  
33 be accommodated in a straightforward way. They also have the benefit of being able to use  
34 epidemiological data directly, as opposed to modelling using summary parameters (e.g.  
35 variance in sexual partner count) abstracted from the data.

36       The principal parameter estimated in epidemiological modelling is that of the basic  
37 reproduction number  $\mathcal{R}_0$ . A historical definition, which must be taken with great care when  
38 applied to complex structured populations, is given by

39       the average number of secondary infections produced when one infected  
40       individual is introduced into a [homogeneously mixed,] wholly susceptible host  
41       population at equilibrium (Anderson & May, 1991).

42 However, though for simple models such as the mean field,  $\mathcal{R}_0$  is well defined, in general no  
43 analytic formula is available for  $\mathcal{R}_0$ . Moreover, one must consider whether the concept of a  
44 single  $\mathcal{R}_0$  value is even appropriate in a complex population (e.g. Green et al., 2009), and  
45 the above definition is not appropriate where the population is not well mixed, or with  
46 correlation between susceptibility and infectiousness.

47       Nevertheless, models of  $\mathcal{R}_0$  and final epidemic size are of utility in considering the  
48 risk of infectious disease between populations with different structure. Various authors have  
49 found that epidemic spread is encouraged or hindered by different network properties. (For  
50 an overview, see Shirley & Rushton, 2005.) A node’s degree – its number of contacts  $k$  – is of  
51 key importance, as is the distribution of contacts: networks with a higher variance of degree  
52 enjoy a higher  $\mathcal{R}_0$  for the same between-node disease transmission rate  $\tau$  (Anderson & May,  
53 1991). Under proportionate mixing, nodes with contact rates  $u$  and  $v$  account for a fraction

54 *uv* of contacts. Deviations from this occur where mixing is preferential: Assortativity in node  
55 degree, with preferential contact between nodes of like degree, increases  $\mathcal{R}_0$  but decreases  
56 final epidemic size (Ghani et al. 1997; Gupta et al. 1989; Anderson et al. 1990; Newman,  
57 2003a). In a broader sense, assortativity occurs wherever there is preferential mixing  
58 according to some node property, e.g. according to sex, with *assortative* mixing in  
59 homosexual and *disassortative* in heterosexual contact networks.

60         In this paper, the network property of most concern is that of clustering. Clustering  
61 measures the degree to which ‘any friend of yours is a friend of mine’. In clustered networks,  
62 if edges  $(a, b)$  and  $(a, c)$  exist, then connections  $(b, c)$  are more likely to exist than would be  
63 expected by chance alone in random networks. This is a form of non-random mixing  
64 associated with both assortativity and spatial structure. Clustered networks have a lower  
65 density of nodes within two steps of a focal node compared with random networks, limiting  
66 the spread of disease and reducing  $\mathcal{R}_0$  (Keeling, 1999; Trapman, 2007; Miller, 2009a), since  
67 nodes infected by the focal node are competing for further neighbouring nodes to infect.

68         Ideally when comparing networks, one would like to be able to vary one parameter  
69 of interest, while keeping all other parameters constant. In this case, we are sure that any  
70 differences in network properties are due to that parameter. In practice, this proves difficult  
71 (Serrano & Boguñá, 2006a; Serrano & Boguñá, 2006b). To explore the dependency of  
72 epidemic dynamics upon network structure imposed by clustering, various authors have  
73 designed different algorithms to generate clustered networks (e.g. Watts & Strogatz, 1998;  
74 Newman, 2003b; Read & Keeling, 2003; Eames, 2007; Kiss & Green, 2008). However, these  
75 algorithms come from quite different start points, and occasionally there are notable  
76 side-effects of clustering upon other network properties (Kiss & Green, 2008).

77         In this paper, we consider a set of previously used algorithms for generating clustered  
78 networks (Newman, 2003b; Read & Keeling, 2003; Eames, 2007) and investigate in what  
79 ways these networks differ with otherwise similar degree and clustering coefficients. Here,  
80 we are primarily interested in parameters of epidemiological interest, in terms of  
81 transmission threshold for epidemic spread, potential epidemic size, and the time-course of  
82 disease; though one must also consider the effect of network structure on the effectiveness  
83 of control strategies (Kiss et al. 2005; Kiss et al. 2008). Some of these properties will be

84 disease or disease model dependent, however properties such as the distribution of shortest  
85 path lengths or departures from proportionate mixing are related. We employ rewiring  
86 algorithms to change the clustering coefficients of networks while maintaining other  
87 selected network properties constant (Kiss & Green, 2008). Particularly, we wish to preserve  
88 the mean degree, degree distribution, and levels of assortative or disassortative mixing.

## 89 **2 Method**

### 90 **2.1 Network construction**

91 A network is described in terms of its number of nodes  $N$  and an adjacency matrix  $A_{ij}$ ,  
92 elements of which are 1 where an edge  $(i, j)$  exists, and zero otherwise. The number of  
93 edges from a single node  $i$  is given by  $k_i = \sum_j A_{ij}$ . All networks were undirected, generated  
94 with  $N = 10\,000$  nodes, with mean node degree of either  $\langle k \rangle = 5$  or  $\langle k \rangle = 10$  and clustering  
95 coefficients chosen from  $\mathcal{C} = 0.2, 0.4, 0.6$  or no clustering  $0.0$ . A set of 100 networks were  
96 generated for each parameter set. The clustering coefficient used is the ratio of triangles to  
97 triples, where triples are permutations of three nodes  $u, v, w$  with edges  $(u, v)$  and  $(u, w)$  and  
98 triangles are those where an additional edge  $(v, w)$  exists. Other definitions of clustering  
99 exist (Watts & Strogatz, 1998), but this measure is easy to calculate and epidemiologically  
100 useful. A selection of different network types were then generated, either using algorithms  
101 reported in the literature, or by rewiring of other networks. These algorithms are described  
102 below.

103 **Fixed degree** Each node has the same number of edges  $k$ , distributed at random by  
104 applying  $50 \times N$  rewiring operations to a lattice network, where in each rewiring  
105 operation four unique nodes with edges  $(a, b)$  and  $(c, d)$  are rewired to give edges  $(a, d)$   
106 and  $(b, c)$ . The number of rewiring operations was greatly in excess of the number of  
107 edges present, and was sufficient that the properties of the rewired networks agreed  
108 with prior expectation.

109 **Poisson** Random Poisson networks were generated by assigning edges  $(a, b)$  for each pair of  
110 nodes  $a < b$  with a single constant probability.

111 **Iterative** An iterative algorithm suggested by Eames (2007) was implemented. This  
 112 algorithm proceeds by repeating two steps. In the first step,  $n_1$  triples are generated by  
 113 connecting unique nodes  $a, b, c$  with edges  $(a, b)$  and  $(a, c)$ . In the second step,  $n_2$   
 114 triangles are generated by selecting a node  $u$  with at least two neighbours at random,  
 115 choosing two random neighbours  $v, w$ , and forming a link  $(v, w)$ . Both steps are  
 116 subject to the constraint that no node may have more than  $k$  connections, and  
 117 duplicate edges are not allowed. The network clustering coefficient is varied by  
 118 changing  $n_1$  and  $n_2$ . Since there is potential for this algorithm to ‘stall’, it is considered  
 119 finished if  $\frac{kN}{2} \times 0.9975$  edges are successfully assigned.

120 **Spatial** This algorithm (Read & Keeling 2003) begins by assigning each node  $i$  coordinates  
 121  $x_i$  and  $y_i$  uniformly distributed across a square world of side-length  $\sqrt{N}$  with toroidal  
 122 boundary conditions (the top and bottom, and left and right edges are adjacent). The  
 123 probability of connection  $p_{ij}$  between two nodes  $i$  and  $j$  is determined by the distance  
 124  $d_{ij}$  between them, according to  $p_{ij} = p_0 \exp(-d^2/2D^2)$  where  $p_0$  and  $D$  are parameters  
 125 to be adjusted to obtain the required  $\langle k \rangle$  and  $\mathcal{C}$ .

126 **Group-based** The clustering algorithm of Newman (2003b) has been discussed by the  
 127 current authors elsewhere (Kiss & Green, 2008). The  $N$  nodes are assigned to ‘groups’  
 128 with connections within groups as described below. Multiple group membership by  
 129 nodes leads to between-group linkages. For each of  $g$  groups,  $\nu$  nodes are chosen at  
 130 random (without replacement), with nodes thus enjoying a mean of  $\mu = gN/\nu$  groups,  
 131 binomially distributed. For every pair of nodes that are members of the same group, an  
 132 edge is added with probability  $p = \frac{k}{\mu(\nu-1)}$  (with higher probability where multiple  
 133 groups are shared). The resulting networks have clustering coefficient  
 134  $\mathcal{C} = \frac{p}{1+\mu(\nu-1)/(\nu-2)}$ , adjusted by altering the number of groups per node,  $\mu$ , subject to  
 135 the constraint that  $p \leq 1$ .

136 **Unclustered** Clustered networks generated by the **iterative** algorithm had clustering  
 137 removed using rewiring as for the **fixed degree** networks.

138 **Unclustered preserving mixing** Alternatively, rewiring to uncluster networks was carried  
 139 out by preserving assortativity. In this case edges  $(u, v)$  and  $(w, x)$  were rewired to

140  $(u, x)$  and  $(w, v)$  only where edges were similar in terms of their node degrees:  $k_u = k_w$   
 141 and  $k_v = k_x$ . This was carried out for the **spatial** algorithm.

142 **Rewire to cluster** Networks created using **fixed degree** or **Poisson** methods were clustered  
 143 using an iterative rewiring algorithm, also recently used by House and Keeling (2010).  
 144 At each iteration, a chain of five random nodes  $u, v, w, x, y$  with edges  $(u, v)$ ,  $(v, w)$ ,  
 145  $(w, x)$ , and  $(x, y)$  was identified (without edges  $(u, y)$  or  $(v, x)$ ) by selecting a node  $u$  at  
 146 random and performing a depth-first search to find suitable chains. The effect of  
 147 rewiring to remove  $(u, v)$  and  $(x, y)$  and insert  $(u, y)$  and  $(v, x)$  edges on a ‘local’  
 148 clustering coefficient is identified (Fig. 1). Where this is increased, the rewiring is  
 149 accepted. The ‘local’ clustering coefficient is defined as the ratio of triangles to triples  
 150 amongst triples  $a, b, c$  where node  $a$  is one of  $u, \dots, y$ . This avoids calculating  
 151 clustering repeatedly for the whole network. A related approach was investigated by  
 152 Bansal et al. (2008).

153 **Reclustered** The **group-based** and **spatial** networks were reclustered to preserve clustering  
 154 coefficients and node degree but remove other forms of structure. This was performed  
 155 by first unclustering, and then using the **rewire to cluster** algorithm to return the  
 156 network to its former clustering coefficient.

157 Small sample networks generated by some of the above procedures are shown in Fig.  
 158 2. To compare the properties of networks with the same level of clustering, generated  
 159 according to different algorithms, we use a series of measures that capture the large scale  
 160 properties of the network.

## 161 2.2 Network measures

162 Simpler network characteristics such as the distribution and average number of contacts  
 163 and, for some cases, degree correlations were kept fixed to focus on the differences in  
 164 large-scale network features. In particular we focus on the measures detailed below:–

165 **Path length** In addition to the adjacency matrix  $A_{ij}$ , we can calculate a matrix of shortest  
 166 path lengths  $L_{ij}$ , denoting the number of edges required to be followed to travel  
 167 through the network from node  $i$  to  $j$ . By definition  $L_{ii} = 0$  and where no connecting

168 path exists,  $L_{ij} = \infty$ . Path lengths were sampled for 10 nodes of each of the 100  
 169 networks in each set.

170 **Correlation dimension** Borrowing a term from chaos theory, we can use the correlation  
 171 sum to describe the large-scale structure of a network (Grassberger & Procaccia,  
 172 1983). We can calculate this in terms of  $L$  as follows:

$$\chi(\varepsilon) = \frac{1}{N^2} \sum_{i,j=1}^N H_1(\varepsilon - L_{ij})$$

173 where  $H_1(x) = 1$  for  $x \geq 0$  and zero for  $x < 0$  (Heaviside step function). Therefore  $\chi$   
 174 represents the proportion of nodes reached within  $\varepsilon$  steps through the network, with  
 175  $\chi(0) = \frac{1}{N}$ ,  $\chi(1) = \frac{\langle k \rangle + 1}{N}$  and  $\chi(\varepsilon)$  increasing for higher  $\varepsilon$  in a manner dependent on  
 176 network structure. If  $\chi(\varepsilon) \propto \varepsilon^\nu$  (i.e. a straight line plot of  $\chi$  v.  $\varepsilon$  on a log-log plot) then  
 177 we consider the network to have dimension  $\nu$ . The shape of  $\chi$  determines the potential  
 178 trajectory of an epidemic on the network.

179 **Mixing measures** We measure the degree to which networks depart from proportionate  
 180 mixing: in assortative networks, there is preferential connection between nodes with  
 181 similar degree. In contrast, in a disassortative network, edges are more likely to  
 182 connect nodes of dissimilar degree than expected with random mixing. Where we  
 183 write  $\sum_{(i,j)} x$  in place of  $\sum_{i,j=1}^N A_{ij}x$ , iterating over all edges  $(i, j) \in E$ , then a measure  
 184 of mixing is given by the following correlation coefficient:

$$r = \frac{M \sum_{(i,j)} k_i k_j - \left( \sum_{(i,j)} k_i \right) \left( \sum_{(i,j)} k_j \right)}{M \sum_{(i,j)} (k_i)^2 - \left( \sum_{(i,j)} k_i \right)^2}$$

185 where  $M = \sum_{i,j=1}^N A_{ij}$ , twice the total number of edges. The correlation  $r$  is positive  
 186 for assortative networks, negative for disassortative, and zero for proportionate  
 187 mixing.

188 **Eigenvalue analysis** The lead eigenvalue  $\lambda$  of the network adjacency matrix can be

189 obtained through simple iteration of the following expression:

$$V^{s+1} = \frac{AV^s}{\|AV^s\|_1},$$

190 iterating until convergence, starting with  $V_i^0 = 1/n$  ( $i = 1 \dots N$ ). The notation  $\|\cdot\|_1$   
 191 indicates that for computational convenience,  $V$  is divided by its total at each step. The  
 192 lead eigenvalue  $\lambda$  is given simply by the solution of  $\lambda V^s = AV^s$  where  $s$  is large. The  
 193 lead eigenvalue is related to  $\mathcal{R}_0$  as discussed below (Diekmann & Heesterbeek, 2000).

194 **Giant connected component (GCC)** A network component is a set of nodes such that a  
 195 path can be found between any pair of nodes within the group. The largest such  
 196 component is the giant connected component (GCC). The potential resilience of a  
 197 network to epidemic spread can be obtained by examining the size of the GCC when a  
 198 proportion of edges are removed at random. Typically, a sharp percolation threshold is  
 199 found, analogous to the epidemic threshold found with increasing transmission rate in  
 200 compartmental models (Newman et al. 2001).

### 201 **2.3 Simulation model**

202 Epidemic simulation allows numerical determination of the effect of network structure on  
 203 the threshold value of the transmission rate for epidemic outbreak, i.e. the point at which  
 204  $\mathcal{R}_0 = 1$ , as well as final epidemic size. The time-course of the spread of disease is also  
 205 obtained.

206 Epidemic dynamics were simulated using an SIR model. At time  $t$ , nodes may be  
 207 susceptible  $S$ , infectious  $I$  or removed  $R$ . Infection is transmitted at rate  $\tau$  across every  
 208  $(S, I)$  edge. The epidemic is seeded with one or more infected nodes. Thereafter, the  
 209 probability of a node becoming infected depends on the state of its neighbouring nodes. In a  
 210 small time interval  $\delta t$ , a node with  $k^I$  infected neighbours becomes infected with probability  
 211  $1 - \exp(-k^I \tau \delta t)$ . Similarly, recovery/removal is modelled as a Poisson process with the  
 212 recovery probability given by  $1 - \exp(-\gamma \delta t)$ , independent of neighbouring nodes. We use  
 213 synchronous updating with  $\gamma = 1$  throughout and a timestep of  $\delta t < 0.01$ , with ten randomly  
 214 selected initial seeding nodes.

## 215 **2.4 Estimates for $\mathcal{R}_0$**

216 **Scope of the problem** Though  $\mathcal{R}_0$  has a simple definition, this simple definition belies a  
 217 range of problems for its calculation and applicability. In addition, for structured  
 218 populations, a distinction can be made between the basic reproduction number of the  
 219 simulated disease  $\mathcal{R}_0$ , and the transmission potential  $\rho_0$  (May & Lloyd, 2001). The latter can  
 220 be defined as the average number of secondary cases derived from an index case chosen at  
 221 random from the population. Unlike  $\mathcal{R}_0$ , it is a function only of the properties of individual  
 222 nodes (see caveat later), and independent of network mixing properties. It is therefore a  
 223 useful baseline for comparison between epidemics with different transmission rates.

224 No general expression for the basic reproductive number  $\mathcal{R}_0$  exists that can be  
 225 directly calculated from basic network properties. Nevertheless, various estimates for  $\mathcal{R}_0$   
 226 have been proposed which encapsulate network structure to a greater or lesser extent.  
 227 Frequently, these are expressed in terms of edge transmissibility  $T = \frac{\tau}{\tau+\gamma}$ : the probability of  
 228 transmission between an isolated  $(S, I)$  pair during the whole infectious period of the  $I$  node  
 229 (Newman, 2002; Green et al. 2006). The estimates described below capture different  
 230 subsets of the network properties listed in the previous sections.

231 **Generation-based approach** In this approach, an estimate of  $\mathcal{R}_0$  is made using the  
 232 distribution of node degrees and correlation between node degrees of adjacent nodes. Thus,  
 233 data concerning the spatial or large-scale network structure and clustering are discarded.  
 234 We consider the *generation* of an infected node to be the number of steps along the infection  
 235 chain it lies from the index case. We let  $I_{i,g}$  denote the number of nodes of degree  $i$  in  
 236 generation  $g$  and  $I_g = \sum_{i=0}^{\infty} I_{i,g}$  is the total number of infected nodes in generation  $g$ . The  
 237 next generation,  $I_{i,g+1}$  is given by

$$I_{i,g+1} = \sum_{j=0}^{\infty} T^j p(i|j) I_{j,g},$$

238 where  $p(i|j)$  is the probability that a node with  $j$  contacts is connected to a node with  $i$   
 239 contacts, and  $T$  is the generation-wide probability of transmission across a link (Kao, 2006).  
 240 Iterating this calculation allows us to determine the number of infected nodes in consecutive  
 241 generations, and based on this, calculate  $\mathcal{R}_0$  (see Appendix 1). Diekmann & Heesterbeek

242 (2000) have shown that under appropriate conditions,  $\mathcal{R}_0$  is given by

$$\mathcal{R}_0 = \lim_{N, n \rightarrow \infty} \left( \prod_{g=1}^n I_{g+1}/I_g \right)^{1/n}.$$

243 In this general case, a closed expression for  $\mathcal{R}_0$  is difficult to obtain, however for specific  
244 networks  $p(i|j)$  can be estimated from the network adjacency matrix as follows:

$$p(i|j) = \frac{\sum_{uv} A_{uv} [k_u = i] [k_v = j]}{\sum_{uv} A_{uv} [k_u = i]},$$

245 where  $[x = y]$  gives unity where  $x = y$ , and zero otherwise. The number of infected nodes in  
246 consecutive generations can then be computed under the assumption of networks of infinite  
247 size with vanishing density of short loops. Recently, Miller (2009) has investigated the  
248 potential for similar formulations for use with clustered networks.

249 **Summary statistics** We now briefly report on various  $\mathcal{R}_0$ -like measures, and how they  
250 relate to the above analytical approach. Assuming random seeding and  $I_0 = 1$ , from the  
251 equations above we obtain a value of  $I_1 = \langle k \rangle T$  (where  $\langle k \rangle$  is the mean number of edges per  
252 node), which corresponds to the transmission potential, written fully as  $\rho_0 = \langle k \rangle \frac{\tau}{\tau + \gamma}$   
253 (Keeling & Grenfell 2000; Green et al. 2006). For a specified  $\rho_0$ , the corresponding  
254 edge-based transmission rate  $\tau$  can be calculated as  $\tau = \gamma \frac{\rho_0}{\langle k \rangle - \rho_0}$  (Green et al. 2006).

255 In the case of proportionate random mixing,  $p(i|j) = ip(i)/\langle k \rangle$ . In this case, it can be  
256 shown that  $I_2 = T^2 \langle k^2 \rangle$  (Appendix 1; Kao, 2006). In general,  $I_{g+1}/I_g$  is constant for any  
257 higher value of  $g$  and therefore  $\mathcal{R}_0 = T \frac{\langle k^2 \rangle}{\langle k \rangle}$ . The calculation should ideally be modified for  
258 undirected networks to account for a node losing a connection upon becoming infected from  
259 its parent case (Andersson, 1998; Kiss et al., 2006). In this, case  $R_0 = T \left( \frac{\langle k^2 \rangle}{\langle k \rangle} - 1 \right)$ . Note  
260 that this correction is not applied to  $\rho_0$ , where infection of the focal node is assumed to  
261 happen ‘by magic’, not infection from a linked node.

262 These expressions account for degree heterogeneity (Anderson & May, 1991), but are  
263 only appropriate where there is no higher-level network structure in the form of clustering  
264 (Keeling, 1999) or assortativity (Anderson et al. 1990). A further measure is given by the  
265 lead eigenvalue of the network adjacency matrix,  $\lambda$  (Diekmann & Heesterbeek, 2000),

266 whose value differs from the previous where the network is broken into dissimilar  
267 components (Green et al., 2009).

### 268 **3 Results**

269 Networks formed through the **iterative** algorithm have a slower increase in  $\chi$  with path  
270 length  $\varepsilon$  and longer mean path lengths, compared to networks with similar parameter  
271 formed through the rewired **fixed-degree** networks (Fig. 3), even for  $\chi(2)$ , which is in a  
272 sense another measure of the degree of local clustering. Examining other network  
273 properties, no difference was found in the levels of clustering at the level of squares  
274 (proportion of quadruples  $a, b, c, d$  with edges  $(a, b)$ ,  $(b, c)$  and  $(c, d)$  that are also squares  
275 with edge  $(a, d)$ ) with coefficients of  $\mathcal{C}_{\square} = 0.44$  and  $0.43$  respectively. However, an interesting  
276 difference was found in the distribution of triangles at the node level (the numbers of triples  
277 being fixed at  $k(k - 1) = 20$ ), with those of the **iterative** networks having lower variance  
278 despite the same mean (17.6 versus 25.3). Local triangle counts were correlated between  
279 connected nodes, but there was no difference in the degree of correlation between network  
280 types ( $r \approx 0.6$ ). That different measures of clustering are not consistent with each other is  
281 not unexpected: the several ‘traditional’ clustering measures (Soffer & Vázquez, 2005)  
282 deviate from each other in different network architectures.

283       The correlation sum of the **spatial** networks alone shows a trend close to a straight  
284 line on the log-log plot (Fig. 3). All other network types show exponential increase (straight  
285 line on semi-log plot, Fig. 3, inset) in proportion of network reached with distance. The  
286 **spatial** networks are therefore the only ones showing finite dimension, and power-law  
287 epidemic spread is expected to be a better model of infection than exponential in epidemics  
288 growing on these networks (Szendrői & Csányi, 2004; see Colgate et al. 1989 for a further  
289 example). With polynomial epidemic growth, there is no exponential growth phase. It is  
290 therefore debatable whether any estimate of  $\mathcal{R}_0$  is appropriate in such cases. The ordering  
291 of the correlation sum plot slopes is reflected in the timescale of epidemic simulations  
292 shown in Fig. 4. In both plots, the slower rise of the **spatial** networks in terms of potential  
293 epidemic spread is seen, even for a particular level of clustering, and a lower rise for the  
294 clustered networks themselves.

295 In network-based models of disease transmission, connected components (CCs) play  
296 an important role (Newman et al., 2001; Newman, 2002; Kenah & Robins, 2007a,b).  
297 Disease seeded into any node in a CC can potentially reach any other node in that  
298 component. Thus, for undirected networks, provided that each link will transmit the  
299 infection, the size of the largest or giant CC (GCC) represents the upper limit for the  
300 potential size of an epidemic. However, for any network only a subset of all edges will be  
301 involved in the transmission process. To account for edges that will not be involved in  
302 disease transmission, the contact network can be de-constructed or diluted by removing a  
303 proportion  $1 - p$  ( $0 \leq p \leq 1$ ) of edges at random (Cohen et al., 2002). This gives rise to a  
304 network that can be regarded as the ‘epidemiological network’ of truly infectious links (Kao  
305 et al., 2006). In contrast with the simulation models discussed elsewhere in this paper, this  
306 is a static approach which does not consider the time-evolution of the epidemic system and  
307 its effects, such as the level of competition for susceptibles between cases and their  
308 secondary cases.

309 The emergence and growth of the GCC can be investigated by increasing the value of  
310  $p$ . In Fig. 5, the size of the GCC is plotted as a function of  $p$  for different network types. For  
311 **spatial** networks with high clustering, the GCC is only present for values of  $p$  that are  
312 considerably higher compared to the case of the re-clustered version of the same network,  
313 the **spatial** network with no clustering, and the unclustered version of the **spatial** network  
314 but with mixing preserved. This indicates that the structure of **spatial** network limits the  
315 epidemic spread and this effect is stronger than for networks with exactly the same level of  
316 clustering but obtained using the **reclustering** algorithm. Similar arguments hold for  
317 networks with **fixed degree**. However, for **group-based** networks the situation changes and  
318 the GCC emerges for smaller values of  $p$  compared to the case of **group-based** networks  
319 with no clustering. In a previous paper Kiss & Green (2008) have shown that this is a direct  
320 consequence of higher clustering leading to higher degree heterogeneity. Although, the GCC  
321 appears for smaller values of  $p$  as clustering increases, its size is limited and stays relatively  
322 small when compared to the unclustered case.

323 For the case of **spatial** networks, in Fig. 6 the cumulative frequency of the CCs is  
324 plotted for below and above percolation regimes. The percolation threshold is given by the

325 value of  $p$  at which the GCC emerges (i.e. when the size of the GCC is comparable to the  
 326 network size in the limit of an infinite network). Here we do not focus on the exact  
 327 percolation threshold but rather on how components grow and connect together to form the  
 328 GCC. Fig. 5(a) illustrates that for unclustered networks, the percolation is sharper with a  
 329 clear transition from having CCs of very small sizes to a single large GCC. However, for high  
 330 levels of clustering ( $\mathcal{C} = 0.6$ ), the transition is less sharp with CCs continuing to grow almost  
 331 independently and only merging in a single large GCC for high values of  $p$  (see Fig. 5(b)).  
 332 This illustrates how clustering promotes the local growth of sub-clusters with few  
 333 inter-cluster links that can lead to a single large component spanning most of the network.

334 In Table 1, numerical estimates for various  $\mathcal{R}_0$ -related quantities are given. Apart  
 335 from the ratio of successive radius perimeters,  $\frac{\chi(2)-\chi(1)}{\chi(1)-\chi(0)}$  (see section *correlation dimension* for  
 336 definition of  $\chi$ ), all measures are based on the assumption of large networks with no loops.  
 337 Moreover,  $\frac{\langle k^2 \rangle}{\langle k \rangle}$  is only valid when networks are proportionally mixed. However, the value of  
 338  $\lambda$  and the generation-based approach captures any departure from proportionate mixing, as  
 339 demonstrated by the positive correlation between these and the mixing measure  $r$ . For the  
 340 **group-based** model, high clustering leads to high contact heterogeneity but no assortativity.  
 341 Contact heterogeneity alone gives larger  $\mathcal{R}_0$  values and a fast spreading epidemic between  
 342 the subset of highly connected nodes. This is reflected in high values of almost all measures.  
 343 The eigenvalue approach does particularly well to capture the low level of assortativity  
 344 generated by high levels of clustering in random or Poisson networks.

## 345 4 Discussion

346 Our results demonstrate that networks exhibiting similar levels of clustering, but generated  
 347 by different algorithms, can differ significantly in their large-scale structure. This has  
 348 implications for the spread of disease on such networks. Moreover, tuning a particular  
 349 network property can lead to undesired but significant changes in network properties other  
 350 than that of interest, and in a different manner for different network construction  
 351 algorithms. This hinders accurate determination of the effect of different network properties  
 352 on the dynamical processes the network supports.

353 To more accurately capture heterogeneity in contact at the level of individuals,

354 models of disease transmission on contact networks – either data based or theoretical – have  
355 become more common. While accurate network data are difficult to collect, many  
356 theoretical network models have been developed simply based on partial information or  
357 general network characteristics (e.g. small-world networks (Watts & Strogatz, 1998) with  
358 short path length and high clustering). Our  $\mathcal{R}_0$ -like parameter estimates above fall into this  
359 category: they are an attempt to summarise the ability of the network to support an  
360 epidemic by extracting partial information from it. The information retained and utilised  
361 varies between measures, and thus so does the applicability of the measure to different  
362 network types. The ability of the measures presented above to capture particular network  
363 properties is summarised in Table 2.

364         The equivalence of various epidemiological network measures is epidemic model- (or  
365 rather, disease) dependent. For example, though we define  $\rho_0$  as the number of secondary  
366 cases from a randomly chosen index case, with exponentially distributed infectious periods  
367 this is in practice an overestimate in individual-based model simulations, since the index  
368 case competes with its own secondary cases (and later) for other secondary cases to infect.  
369 The same principle applies to  $\mathcal{R}_0$ . This effect is present in our network simulations as well as  
370 the mean-field model (Appendix 2) and is particularly strong in clustered networks and a  
371 large seeding population, but absent in discrete generation-based models.

372         Many assumptions are implicit in formulations of network epidemic models such as  
373 that presented above. For example, we assume that all edges have equal weight and that  
374 this is not affected by the number of connections an individual makes, as might be the case  
375 under the frequency dependent model paradigm. Other measures of clustering giving  
376 different weightings to nodes with dissimilar  $k$  may be more appropriate for other network  
377 types. We also assume exponentially distributed infectious period lengths, a distribution  
378 with a long tail and thus much overlap of generations of infection. With many such other –  
379 often more biologically appropriate – approaches available, there is always the danger of  
380 letting ‘the tail wag the dog’, that is being driven by what we usually model, rather than  
381 being driven by modelling epidemic problems that need solutions.

382         Simple analytical approaches can aid the analysis of complex networks. For example,  
383 Newman (2002) showed that under some appropriate conditions the transmission of

384 diseases on networks is equivalent to a bond-percolation problem with the possibility to  
385 analytically or semi-analytically compute outbreak threshold and outbreak size distribution.  
386 Kenah & Robins (2007 a, b) have later on expanded on the precise conditions for such an  
387 agreement between the two approaches to hold. Using a similar approach, Miller (2007)  
388 considered the more general case of varying susceptibility and infectivity. However, all these  
389 approaches are based on the assumptions of infinite networks with no loops and in some  
390 cases proportionate or random mixing. Recently, Newman (2009) and Miller (2009b)  
391 developed an approach for analytic calculations of many properties in a class of random  
392 clustered networks and confirmed previous findings based on simulation. Britton et al.  
393 (2008) used a branching process approximation to study the spread of an epidemic on a  
394 network with tunable clustering. Their analytical results for the epidemic threshold and the  
395 probability of a large outbreak on clustered networks confirm in a rigorous way the effect of  
396 clustering on the spread of epidemics. Even though such models are difficult to extend to  
397 networks with more heterogeneity or structure, such simple theoretical models provide a  
398 useful starting point for investigating the effect of any departure from the idealized network  
399 models.

400       Clustering is a local property and the triangular sub-graph structure and their  
401 frequency has been generalised to *motifs* (e.g. four nodes in a line or connected in a circle),  
402 widely studied in the context of red systems biology (Milo et al., 2002). For example, for  
403 gene regulatory networks, certain motifs are more abundant in the network compared to  
404 what would be expected at random and these frequently re-occurring small structures are  
405 regarded as the building block of networks. For our particular case, different  
406 network-generating algorithms could lead to more frequently observing motifs composed of  
407 four or more nodes. However, we found no difference in clustering at the level of squares  
408 between **iterative** and **fixed-degree** networks. Future work could examine the presence and  
409 frequency other larger motifs that could be a by-product of the generating algorithms and  
410 could have significant effect on disease transmission.

411       An important aspect of many disease transmission models is the exploration of the  
412 efficacy of different control measures. For example, previous studies have shown that this  
413 strongly depends on disease characteristics and contact network properties: Contact tracing

414 performs better on clustered networks (Eames & Keeling 2003; Kiss et al., 2005) where the  
 415 redundant local links offer multiple opportunities to trace and isolate individuals who have  
 416 been in contact with infectious individuals. Similarly, with STIs on assortatively mixed  
 417 networks, contact tracing must be performed quickly or at least at a level that is comparable  
 418 to the rate of disease transmission (Kiss et al, 2008). Such studies are often based on  
 419 theoretical network models and focus on investigating the effect of a particular network  
 420 property. In this paper we have shown that theoretical network models must be used with  
 421 care and that the analysis of the network itself merits as careful consideration as the  
 422 dynamical processes that the networks support. Combining network measures that focus on  
 423 local node properties with large-scale network measures can improve the transparency and  
 424 accuracy of modelling predictions.

## 425 5 Appendices

### 426 5.1 Generation-based network approach

427 Following on from the main text, where we let  $I_{i,g}$  denote the number of infected nodes of  
 428 degree  $i$  in generation  $g$ ,  $I_{i,g+1}$  is given by

$$I_{i,g+1} = \sum_{j=0}^{\infty} T j p(i|j) I_{j,g},$$

429 where  $p(i|j)$  is the probability that a node with with  $j$  contacts is connected to a node with  $i$   
 430 contacts. In the case of proportionate random mixing,  $p(i|j) = ip(i) / \langle k \rangle$ . Hence, given  
 431 random seeding of initial cases in the zeroth generation such that  $I_{j,0} = p(j)$ , the number of  
 432 individuals with degree  $i$  in the first generation is

$$I_{i,1} = \sum_j T j \frac{ip(i)}{\langle k \rangle} I_{j,0} = \frac{Tip(i) \sum_j jp(j)}{\langle k \rangle} = Tip(i)$$

433 while in the second generation this is

$$I_{i,2} = \sum_j T j \frac{ip(i)}{\langle k \rangle} I_{j,1} = \frac{T^2 ip(i) \sum_j j^2 p(j)}{\langle k \rangle} = \frac{T^2 \langle k^2 \rangle}{\langle k \rangle} ip(i).$$

434 Summation according to  $i$  gives  $I_1 = T \langle k \rangle$  and  $I_2 = T^2 \langle k^2 \rangle$ . Dividing  $I_2$  by  $I_1$  we obtain the  
 435 standard estimate for  $\mathcal{R}_0$ .

## 436 5.2 Generation-based mean-field model

437 The mean-field SIR model can be posed in a way in which the generations of infection may  
 438 be identified. The infected compartment  $I$  is subdivided into compartments indexed by the  
 439 generation of infection  $g \in \mathbb{N}_0$ . Infection by generation  $g$  produces infected individuals at  
 440 generation  $g + 1$ , with therefore no flow into the  $g = 0$  index case compartment. As usual,  $\beta$   
 441 and  $\gamma$  represent the infection and removal rates.

$$\begin{aligned} \frac{dI_g}{dt} &= \beta S I_{g-1} - \gamma I_g & g > 0 \\ \frac{dI_g}{dt} &= -\gamma I_g & g = 0 \\ \frac{dS}{dt} &= -\beta \sum_g I_g \\ \frac{dR_g}{dt} &= \gamma I_g \end{aligned}$$

442 Solving this model for  $\beta = 3$  and  $\gamma = 1$ , and an initial infected population of  $I_{0,0} = 0.0001$ ,  
 443 we obtain a final state of  $R_{1,\infty} = 0.000295$ , suggesting a value of  $\mathcal{R}_0 = 2.95$ , less than the  
 444 theoretical value of  $\mathcal{R}_0 = \beta/\gamma = 3$ . This theoretical value is approached as  $I_{0,0}$  approaches  
 445 zero.

## 446 References

- 447 Anderson, R.M., & Garnett, G. (2000). Mathematical models of the transmission and  
 448 control of sexually transmitted disease. *Sex. Transm. Dis.* 27: 636 – 643.
- 449 Anderson, R.M., Gupta, S. & Ng, W. (1990). The significance of sexual partner contact  
 450 networks for the transmission of HIV. *J. AIDS* 3: 417 – 429.
- 451 Anderson, R.M. & May, R.M. (1991). *Infectious Diseases of Humans: Dynamics and*  
 452 *Control*. Oxford University Press, Oxford.
- 453 Andersson, H. (1998). Limit theorems for a random graph epidemic model. *The Annals of*  
 454 *Applied Probability* 4: 1331 – 1349.
- 455 Bansal, S., Khandelwal, S. & Meyers, L.A. (2008). Evolving clustered random networks.  
 456 arXiv:0808.0509

- 457 Britton, T., Deijfen, M., Lagerås, A.N. & Lindholm, M. (2008) Epidemics on random  
458 graphs with tunable clustering. *J. Appl. Probab.* 45: 743 – 756.
- 459 Cohen, R., Ben-Avraham, D. & Havlin, S. (2002) Percolation critical exponents in  
460 scale-free networks. *Phys. Rev. E.* 66: 036. 113.
- 461 Colgate, S.A., Stanley, E.A., Hymen, J.M., Layne, S.P. & Qualls, C. (1989). A risk behaviour  
462 based model of the cubic growth of AIDS in the United States. *Int. Conf. AIDS* 5: 61.
- 463 Diekmann, O. & Heesterbeek, J.A.P. (2000). *Mathematical epidemiology of infectious  
464 diseases: model building, analysis and interpretation.* Wiley, Chichester, UK.
- 465 Eames, K.T.D. & Keeling, M.J. (2003). Contact tracing and disease control. *Proc. R. Soc. B*  
466 270: 2565 – 2571.
- 467 Eames, K.T.D. (2007). Modelling disease spread through random and regular contacts in  
468 clustered populations. *Theor. Pop. Biol.* 73: 104 – 111.
- 469 Ghani, A., Swinton, J., & Garnett, G. (1997). The role of sexual partnership networks in  
470 the epidemiology of gonorrhoea. *Sex. Transm. Infect.* 24: 45 – 56.
- 471 Grassberger, P. & Procaccia, I. (1983). Measuring the strangeness of strange attractors.  
472 *Physica 9D*: 189 – 208.
- 473 Green, D.M., Gregory, A., & Munro, L.A. (2009). Small- and large-scale network structure  
474 of live fish movements in Scotland. *Prev. Vet. Med.* in press.
- 475 Green, D.M., Kiss, I.Z., & Kao, R.R. (2006). Parameterisation of Individual-Based Models:  
476 Comparisons with Deterministic Mean-Field Models. *J. Theor. Biol.* 239: 289 – 297.
- 477 Gupta, S., Anderson, R.M., & May, R.M. (1989). Networks of sexual contacts: implications  
478 for the pattern of spread of HIV. *AIDS* 3: 807 – 818.
- 479 House, T. & Keeling, M.J. (2010). The impact of contact tracing in clustered populations.  
480 *PLoS Computational Biology* 6: e1000721.
- 481 Kao, R.R. (2006). Evolution of pathogens towards low  $\mathcal{R}_0$  in heterogeneous populations.  
482 *J. Theor. Biol.* 242: 634 – 642.
- 483 Kao, R.R., Danon, L., Green, D.M. & Kiss, I.Z. (2006) Demographic structure and  
484 pathogen dynamics on the network of livestock movements in Great Britain. *Proc. R.  
485 Soc. Lond. B* 273: 1999 – 2007.
- 486 Kenah, E. & Robins, J.M. (2007a). Second look at the spread of epidemics on networks.  
487 *Phys. Rev. E* 76: 036113.
- 488 Kenah, E. & Robins, J.M. (2007b). Network-based analysis of stochastic SIR epidemic  
489 models with random and proportionate mixing. *J. Theor. Biol.* 249: 706 – 722.
- 490 Keeling, M.J. (1999). The effects of local spatial structure on epidemiological invasions.  
491 *Proc. R. Soc. Lond. B* 266: 859 – 867.
- 492 Keeling, M.J. & Grenfell, B.T. (2000). Individual-based perspectives on  $R_0$ . *J. Theor. Biol.*  
493 203: 51 – 61.
- 494 Kiss, I.Z., Green, D.M. & Kao, R.R. (2005). Disease contact tracing in random and  
495 clustered networks. *Proc. R. Soc. Lond. B* 272: 1407 – 1414.

- 496 Kiss, I.Z., Green, D.M. & Kao, R.R. (2006). The effect of network heterogeneity and  
497 multiple routes of transmission on final epidemic size. *Math. Biosci.* 203: 124 – 136.
- 498 Kiss, I.Z. & Green, D.M. (2008). Comment on ‘Properties of highly clustered networks’.  
499 *Phys. Rev. E* 78: 048101.
- 500 Kiss, I.Z., Green, D.M. & Kao, R.R. (2008). The effect of network mixing patterns on  
501 epidemic dynamics and the efficacy of disease contact tracing. *J. R. Soc. Interface* 5:  
502 791 – 799.
- 503 May, R.M. & Lloyd, A.L. (2001). Infection dynamics on scale-free networks. *Phys. Rev. E*  
504 64: 066112.
- 505 Miller, J.C. (2007). Epidemic size and probability in populations with heterogeneous  
506 infectivity and susceptibility. *Phys. Rev. E* 76: 010101(R).
- 507 Miller, J.C. (2009a). Spread of infectious disease through clustered populations. *J. Roy.*  
508 *Soc. Interface* 6: 1121 – 1134.
- 509 Miller, J.C. (2009b). Percolation and epidemics in random clustered networks. *Phys. Rev.*  
510 *E* 80: 020901(R).
- 511 Milo, R., Shen-Orr, S., Itzkovitz, S., Kashtan, N., Chklovskii, D. & Alon, U. (2002).  
512 Network motifs: simple building blocks of complex networks. *Science* 298: 824 – 827.
- 513 Newman, M. E. J., Strogatz, S. H. & Watts, D. J. (2001) Random graphs with arbitrary  
514 degree distribution and their applications. *Phys. Rev. E* 64: 026 118.
- 515 Newman, M.E.J. (2002). The spread of epidemic disease on networks. *Phys. Rev. E* 66:  
516 016128.
- 517 Newman, M.E.J. (2003a). Mixing patterns in networks. *Phys. Rev. E* 67: 026126.
- 518 Newman, M.E.J. (2003b). Properties of highly clustered networks. *Phys Rev. E* 68:  
519 026121.
- 520 Newman, M.E.J. (2009). Random graphs with clustering. *Phys. Rev. Lett.* 103: 058701.
- 521 Read, J.M. & Keeling, M.J. (2003). Disease evolution on networks: the role of contact  
522 structure. *Proc. R. Soc. Lond. B* 270: 699 – 708.
- 523 Serrano, M.A. & Boguñá, M. (2006a). Percolation and epidemic thresholds in clustered  
524 networks. *Phys. Rev. Lett.* 97: 088701.
- 525 Serrano, M.A. & Boguñá, M. (2006b). Clustering in complex networks. II. Percolation  
526 properties. *Phys. Rev. E* 74: 056115.
- 527 Szendrői, B. & Csányi, G. (2004) Polynomial epidemics and clustering in contact  
528 networks. *Proc. R. Soc. Lond. B (Suppl.)* 271, S364 ?- S366.
- 529 Shirley, M.D.F. & Rushton, S.P. (2005). The impacts of network topology on disease  
530 spread. *Ecological Complexity* 2: 287 – 299.
- 531 Soffer & S.N., Vázquez, A. (2005). Network clustering coefficient without  
532 degree–correlation biases. *Phys. Rev. E* 71, 057 101.

- 533 Trapman, P. (2007). On analytical approaches to epidemics on networks. *J. Theor. Biol.*  
534 71: 160 – 173.
- 535 Watts, D.J. & Strogatz, S.H. (1998). Collective dynamics of ‘small-world’ networks.  
536 *Nature* 393: 440 – 442.

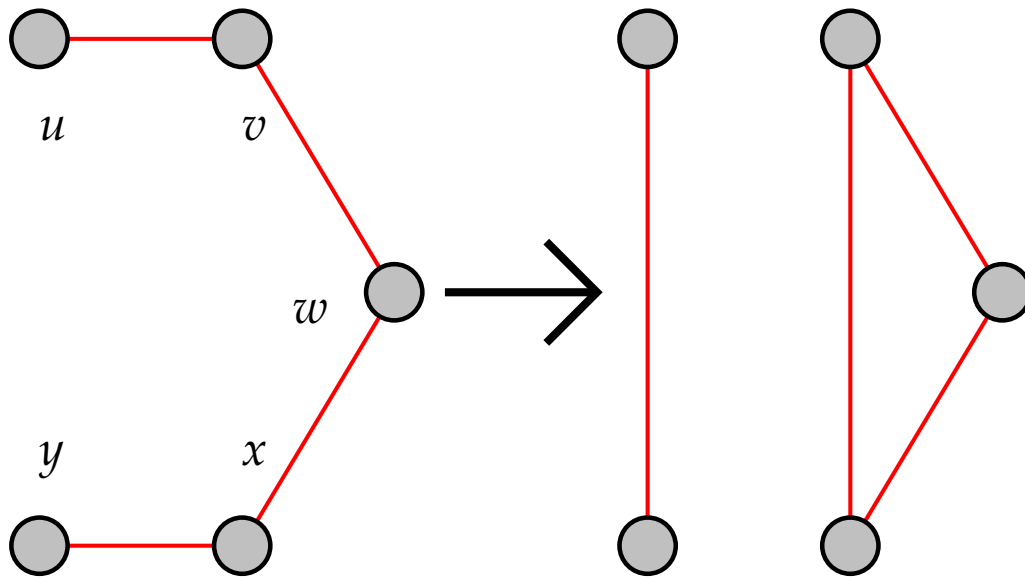
537 **Display items**

Figure 1: Rewiring algorithm step for generating clustering.

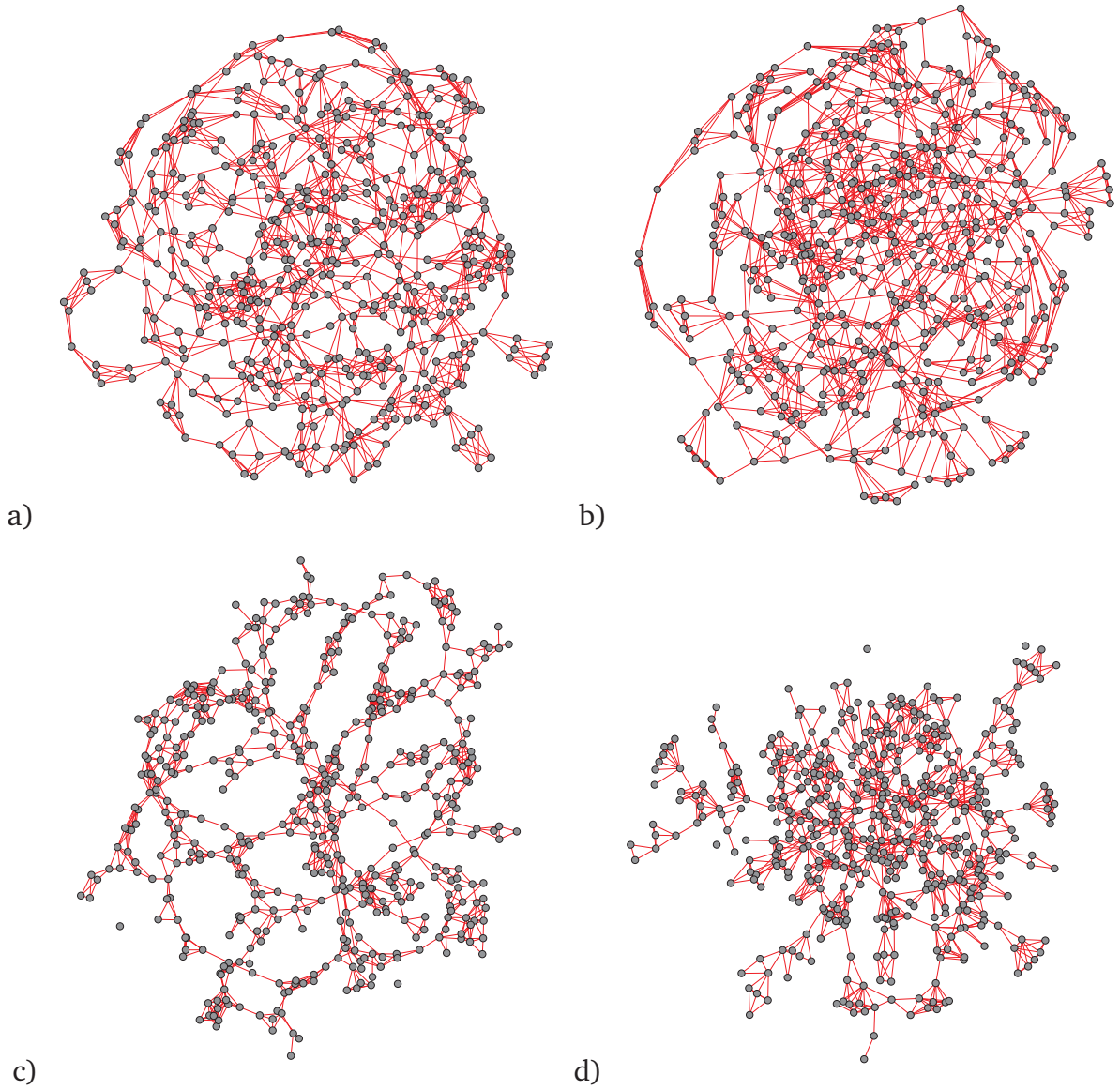


Figure 2: Sample networks with  $N = 500$ ,  $\langle k \rangle = 5$  and  $C = 0.6$ . a) **iterative** algorithm; b) **rewire to cluster** from constant  $k$ ; c) **spatial** and d) this network **reclustered**.

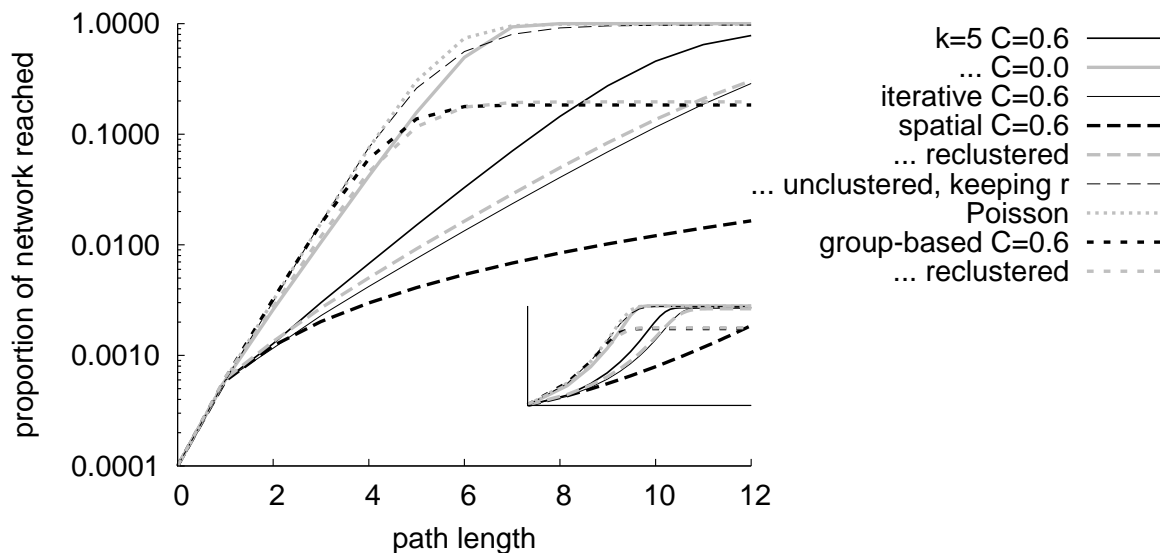


Figure 3: Correlation sum for different clustering algorithms. Inset shows same figure on a log-log scale. All lines are thick unless otherwise stated. Solid black line: fixed degree  $C = 0.6$ ; solid grey: fixed degree  $C = 0$ ; thin solid: iterative  $C = 0.6$ ; black dashed: spatial  $C = 0.6$ ; grey dashed: spatial reclustered  $C = 0.6$ ; thin dashed: spatial unclustered preserving mixing; grey dotted: Poisson; black short dash: group-based  $C = 0.6$ ; grey short dash: group-based reclustered  $C = 0.6$ .  $\langle k \rangle = 5$  throughout.

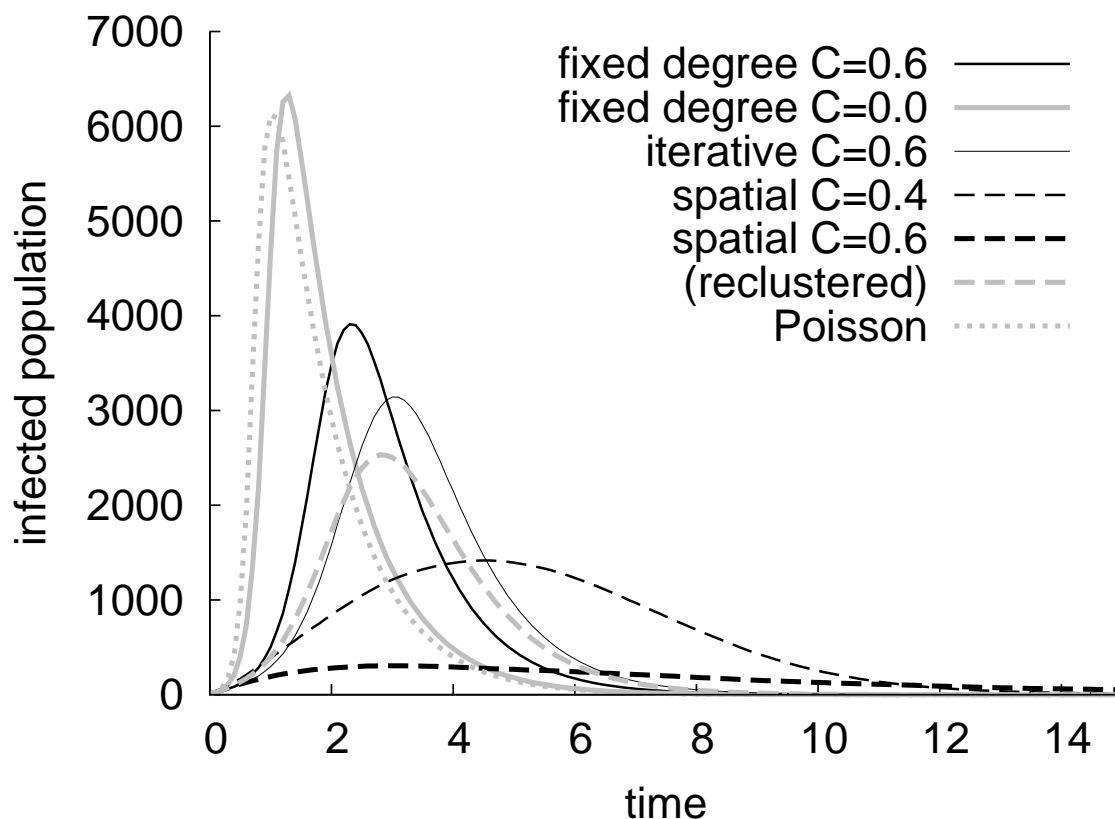


Figure 4: Time series for simulated epidemic. Results are mean prevalence for 10 simulations on each of 25 networks, with  $\tau = 2.5$  and  $\gamma = 1$ . Line styles, mostly as in figure 3, are shown in the legend; throughout,  $\langle k \rangle = 5$ .

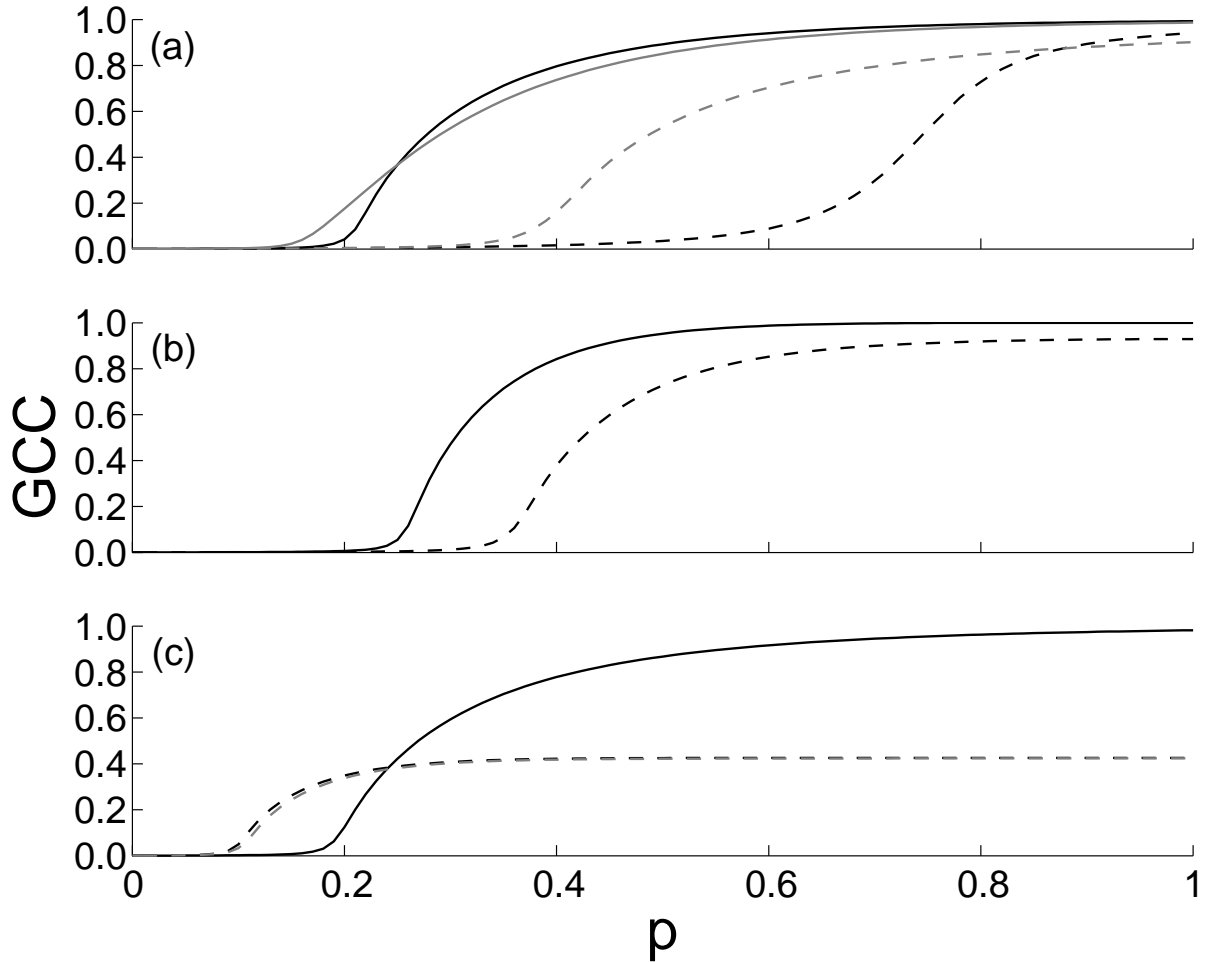


Figure 5: The size of the giant connected component (GCC) for increasing probability  $p$  of links being present. (a) spatial  $\mathcal{C} = 0$  (black continuous),  $\mathcal{C} = 0.6$  (black dashed), reclustered  $\mathcal{C} = 0.6$  (grey dashed) and unclustered preserving mixing (grey continuous), (b) fixed degree  $\mathcal{C} = 0$  (black continuous) and  $\mathcal{C} = 0.6$  (black dashed), and (c) group-based  $\mathcal{C} = 0$  (black continuous),  $\mathcal{C} = 0.6$  (black dashed) and reclustered  $\mathcal{C} = 0.6$  (grey dashed). All simulations based on networks with  $\langle k \rangle = 5$ .

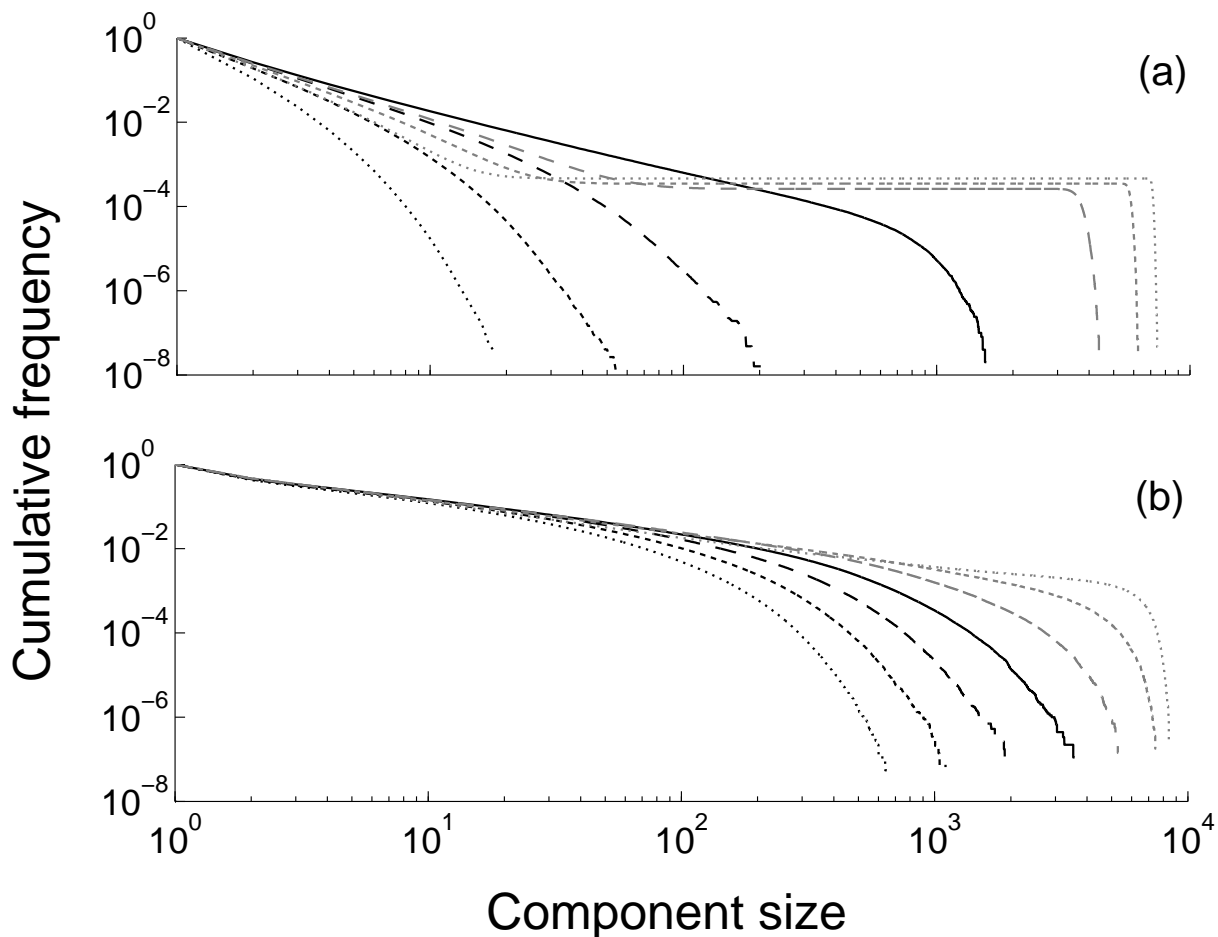


Figure 6: Cumulative distribution of the connected component size for the spatial network model with  $c = 0.0$  (a) and  $c = 0.6$  (b). Results are based on the outcome of 10000 simulations (100 simulations on 100 different networks). (a) Below percolation for  $p = 0.05, 0.1, 0.15, 0.2$  (black: dotted, short dashed, long dashed and solid) and above percolation for  $p = 0.25, 0.3, 0.35$  (grey: long dashed, short dashed, dotted). (b) Below percolation for  $p = 0.45, 0.5, 0.55, 0.6$  (black: dotted, short dashed, long dashed and solid) and above percolation for  $p = 0.65, 0.7, 0.75$  (grey: long dashed, short dashed, dotted). All simulations based on networks with  $\langle k \rangle = 5$ .

Table 1: Basic statistics of constructed networks for  $\langle k \rangle = 5$ . Clustering coefficient  $\mathcal{C}$ , mixing measure  $r$ , ratio of degree distribution first two moments  $\frac{\langle k^2 \rangle}{\langle k \rangle}$ , lead Eigenvalue of adjacency matrix  $\lambda$ , ratio of nodes within two and one step from focal node (ratio of successive radius perimeters)  $\frac{\chi(2)-\chi(1)}{\chi(1)-\chi(0)}$ , and the next-generation matrix estimate  $\mathcal{R}_0 \sim \frac{I_2}{I_1}$  are shown.

Network	$\mathcal{C}$	$r$	$\frac{\langle k^2 \rangle}{\langle k \rangle}$	$\lambda$	$\frac{\chi(2)-\chi(1)}{\chi(1)-\chi(0)}$	$\frac{I_2}{I_1}$
Fixed degree	0.00	–	5.0	5.0	4.0	5.0
Fixed degree, clustered	0.60	–	5.0	5.0	1.4	5.0
Iterative, clustered	0.61	–	5.0	5.0	1.1	5.0
	0.21	–	5.0	5.0	3.0	5.0
Spatial, clustered	0.58	0.583	6.0	11.0	1.3	7.2
Spatial, reclustered	0.60	0.072	6.0	7.8	1.4	6.1
... unclustered preserving mixing	0.00	0.583	6.0	8.9	4.9	7.2
Spatial, no clustering	0.00	0.000	6.0	6.2	5.0	6.0
Group-based, clustered	0.61	0.000	14.0	14.7	5.0	14.0
Group-based, unclustered	0.01	0.000	6.5	6.7	5.4	6.5
Poisson, clustered	0.60	0.072	6.0	7.8	1.5	6.0
	0.40	0.030	6.0	6.9	2.6	6.0
	0.20	0.007	6.0	6.3	3.8	6.0
... no clustering	0.00	0.000	6.0	6.2	5.0	6.1

Table 2: Sensitivity of network measures to network properties (see caption to Table 1 for definitions). A tick indicates the indicated measure is sensitive to differences in the indicated network property.

Property	$\langle k \rangle$	$\frac{\langle k^2 \rangle}{\langle k \rangle}$	$\lambda$	$\frac{\chi(2)-\chi(1)}{\chi(1)-\chi(0)}$	$\frac{I_2}{I_1}$	simulation
Degree	✓	✓	✓	✓	✓	✓
Degree heterogeneity		✓	✓	✓	✓	✓
Clustering				✓		✓
Overlap of generations						✓
Non-random mixing			✓	✓	✓	✓
Community structure			✓			✓